Stem Cell Reports
Report
OPEN ACCESS

Extracellular Vesicles Derived from Osteogenically Induced Human Bone Marrow Mesenchymal Stem Cells Can Modulate Lineage Commitment

Margarida Martins,[1,2] Diana Ribeiro,[1,2] Albino Martins,[1,2] Rui Luís Reis,[1,2] and Nuno Meleiro Neves[1,2,*]
[1]3B's Research Group-Biomaterials, Biodegradable and Biomimetics, University of Minho, Headquarters of the European Institute of Excellence on Tissue Engineering and Regenerative Medicine, Avepark, Barco, 4805-017 Guimarães, Portugal
[2]ICVS/3B's PT Government Associated Laboratory, Braga/Guimarães, Portugal
*Correspondence: nuno@dep.uminho.pt
http://dx.doi.org/10.1016/j.stemcr.2016.01.001

SUMMARY

The effective osteogenic commitment of human bone marrow mesenchymal stem cells (hBMSCs) is critical for bone regenerative therapies. Extracellular vesicles (EVs) derived from hBMSCs have a regenerative potential that has been increasingly recognized. Herein, the osteoinductive potential of osteogenically induced hBMSC-EVs was examined. hBMSCs secreted negatively charged nanosized vesicles (~35 nm) with EV-related surface markers. The yield of EVs over 7 days was dependent on an osteogenic stimulus (standard chemical cocktail or *RUNX2* cationic-lipid transfection). These EVs were used to sequentially stimulate homotypic uncommitted cells during 7 days, matching the seeding density of EV parent cells, culture time, and stimuli. Osteogenically committed hBMSC-EVs induced an osteogenic phenotype characterized by marked early induction of *BMP2*, *SP7*, *SPP1*, *BGLAP*/*IBSP*, and alkaline phosphatase. Both EV groups outperformed the currently used osteoinductive strategies. These data show that naturally secreted EVs can guide the osteogenic commitment of hBMSCs in the absence of other chemical or genetic osteoinductors.

INTRODUCTION

Human bone marrow mesenchymal stem cells (hBMSCs) are attractive candidates for advanced cell therapies, including bone regeneration (Costa-Pinto et al., 2012). Satisfactory treatments are hampered by the difficulty in obtaining a well-defined population of terminally differentiated cells. This causes heterogeneity of hBMSCs, enhances the possibility of spontaneous differentiation into other lineages (Nombela-Arrieta et al., 2011), and may shorten the cells' engraftment-activation time (Tsubota et al., 1999). Therefore, approaches beyond the standard chemical cocktails have been investigated (Heng et al., 2004) such as genetic modulation through the overexpression of genes (e.g., runt-related transcription factor 2, *RUNX2*) (Karsenty et al., 2009; Monteiro et al., 2014), and the use of synthetic/recombinant factors such as bone morphogenetic protein 4 or cell-derived conditioned medium (CM). Indeed, CM contains an array of growth factors, cytokines, proteins (Makridakis et al., 2013), and the recently highlighted extracellular vesicles (EVs) (Collino et al., 2010). EVs are nanosized particles (exosomes, 30–100 nm; microvesicles, 50–2000 nm) carrying lipids, proteins, and nucleic acids (Akers et al., 2013). It has been suggested that hBMSC-secreted EVs include differentiation cues (miRNA, Collino et al., 2010; Baglio et al., 2015; tRNA, Baglio et al., 2015; and proteins, Kim et al., 2012), even upon osteogenic induction (Xu et al., 2014). The regenerative potential of MSC-EVs is supported by preclinical studies showing the improvement of at least one clinical outcome associated with acute kidney/liver/lung injury, myocardial infarction, or hindlimb ischemia (Akyurekli et al., 2015). Furthermore, the literature shows that hBMSCs undergo osteogenic differentiation induced by EVs derived from monocytes (Ekstrom et al., 2013) or platelet lysate (Torreggiani et al., 2014). These data enable us to hypothesize that EVs may be vehicles of communication toward tissue regeneration. The knowledge on the bone regenerative potential of hBMSC-EVs is scarce. Therefore, the purpose of this study is to validate the functionality of hBMSC-EVs in the osteoinduction of hBMSCs. We hypothesized that if EVs mirror the content and fate of parent cells, then EVs derived from osteogenically committed hBMSCs will induce the osteogenic commitment of homotypic cells without further supplementation.

RESULTS

hBMSCs Exposed to Osteogenic Stimuli Secrete EVs during Culture

hBMSCs were induced into the osteogenic lineage over 7 days by continuous chemical stimuli provided by standard osteogenic medium (OM) (Jaiswal et al., 1997) or by a single genetic stimulus in basal medium (RUNX-2). We next isolated EVs from the CM of chemically and genetically induced hBMSCs (OM-EVs and RUNX2-EVs, respectively) at specific time points using polymeric precipitation.

EVs showed a polydisperse size distribution by dynamic light scattering (Figure 1A), with polydispersity indexes between 0.15 and 0.6 (min and max), independently of the culture conditions and time. The main peak corresponded to ≥65% of the population (65.2%–88%, 68.7%–73.5%, 76.2%–84%, min-max for OM-, RUNX2-, basal medium [BM]-EVs, respectively). Within this population, the diameter of EVs was very homogeneous (31.9–40.2 nm), irrespective of culture time or stimulus (Figure 1B). In contrast, the size of EVs within the second peak (Figure 1A) ranged between 45 and 348.6 nm. These findings were corroborated by atomic force microscopy, which showed a population of intact rounded structures with estimated desiccated diameters of 32, 40, and 24 nm (Figure 1C, a–c). On the other hand, as assessed by laser Doppler micro-electrophoresis, the surface charge of OM-, RUNX2-, and BM-EVs averaged at −5.2, −6.4, and −5.9 mV, respectively, and was similar within the different groups (Figure 1B).

To shed light into the biochemical profile of EVs, we first used flow cytometry (Figure 1D) to detect the tetraspanins CD9/63/81, expected to be enriched in EVs fractions (Lötvall et al., 2014). These analyses showed that EVs labeled for each of the markers show a distinct positive shift of the fluorescence signal beyond the non-labeled controls. Furthermore, the data suggested abundant CD81-positive and weak CD9-positive EVs populations, despite the culture conditions (Figure 1D). The presence of CD63-positive EVs was further confirmed using ELISA (Figure 1E).

In addition, we aimed at estimating the release of EVs during culture, based on the normalized number of CD63 particles and total EV protein (Figure 1E). An osteogenic stimulus-dependent release was observed, differing from that observed in control conditions. Specifically, while for OM cultured cells the release of EVs remained at a steady level over time, for RUNX2 stimulated cells the secretion of EVs, in terms of total protein, increased over time peaking from the fifth day of culture onward (day 3 versus 5 or versus 7, $p < 0.01$; Figure 1E).

Collectively, these results show that hBMSCs secrete populations of nanosized particles with physical and biochemical features of EVs, and the yield is regulated by the osteogenic stimulus provided.

hBMSCs Osteogenically Derived EVs Outperform Current Strategies to Elicit hBMSCs Osteogenic Commitment

To test our hypothesis, OM- and RUNX2-EVs were isolated at set time points during culture (Figure 1E) and used to sequentially feed uncommitted homotypic hBMSCs, matching seeding density, culture time, and stimuli without further supplementation. Therefore, the concentration of EVs added to culture mimicked the specific release of parent cells into the CM.

We first assessed whether EVs could interact and deliver nucleic acids to homotypic recipient cells. RUNX2-EVs isolated from 1-day cultured cells expressing *RUNX2-GFP* tag, were added to uncommitted hBMSCs. After 1 day, the *GFP* expression was on average 233-fold greater versus BM in cells exposed to RUNX2-EVs (6.8–803, min-max), although at lower levels than that observed for parent cells transfected by lipofection (average 1.6×10^6 fold change, 4×10^4–7×10^6, min-max). This suggests that EVs are able to interact with the recipient cells and transfer functional plasmid DNA.

The ability of OM- and RUNX2-EVs to promote the onset of osteogenesis was examined and compared with currently available strategies. The differentiation process is known to impair cell proliferation, due to an increase in the length of the cell cycle (Roccio et al., 2013), and to induce changes in the protein synthesis rate (Kristensen et al., 2013). Therefore, we evaluated the profile of recipient hBMSC proliferation (Figure 2A) and total protein (Figure 2B). Notably, a high seeding density was used to ensure high transfection efficiency. Under these conditions, the proliferation capacity of OM-EV-treated cells decreased after day 3 versus BM and OM (Figure 2A), in parallel with a net protein increase (day 5, versus BM) (Figure 2B). Furthermore, RUNX2-EV treatment did not impair cell proliferation versus BM, in contrast to parent cells (RUNX2), attaining proliferation levels higher than those of parent and OM-EV-exposed cells at the seventh day (Figure 2A), without major changes in total protein (Figure 2B).

The osteoinductive potential of EVs was then evaluated in terms of the expression of the extracellular matrix marker alkaline phosphatase (ALP) (Figure 2C). OM- and RUNX-2 EVs induced early activation of ALP, in contrast to that exhibited by the parent cells. Notably, this was observed in the absence of the mineralization inductors dexamethasone and β-glycerophosphate (Langenbach and Handschel, 2013). To better define the osteogenic commitment of these cells, the temporal gene expression of osteogenic markers was investigated (Figure 3). OM-EV-cultured hBMSCs showed early overexpression of the activator bone morphogenetic protein 2 (*BMP2*) (Figure 3C) by ~3- to 6-fold versus BM and OM, and a transient increase in the expression of the Sp7 transcription factor (osterix) (*SP7*) (Figure 3B) by 6-fold versus BM at day 3. Indeed, osteoblastic differentiation is determined by the overexpression of *SP7* (Sinha and Zhou, 2013) through the BMP-2 signaling cascade (Ulsamer et al., 2008). Herein, the data suggest early activation of the cascade independent of the upstream factor *RUNX2*. In addition, at early culture times, the downstream factors secreted phosphoprotein 1 (osteopontin) (*SPP1*) (Figure 3D) and

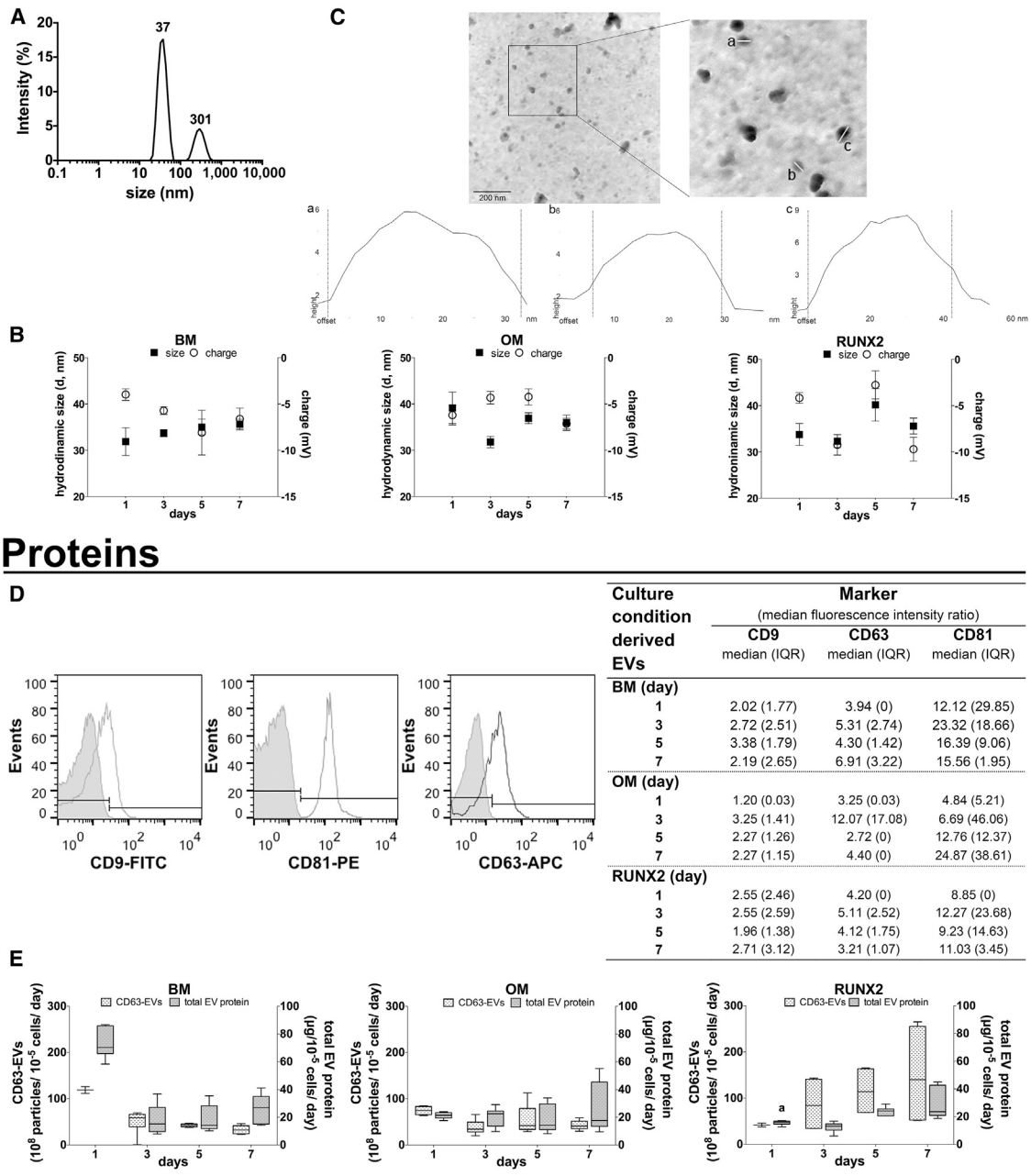

Culture condition derived EVs	Marker (median fluorescence intensity ratio) CD9 median (IQR)	CD63 median (IQR)	CD81 median (IQR)
BM (day)			
1	2.02 (1.77)	3.94 (0)	12.12 (29.85)
3	2.72 (2.51)	5.31 (2.74)	23.32 (18.66)
5	3.38 (1.79)	4.30 (1.42)	16.39 (9.06)
7	2.19 (2.65)	6.91 (3.22)	15.56 (1.95)
OM (day)			
1	1.20 (0.03)	3.25 (0.03)	4.84 (5.21)
3	3.25 (1.41)	12.07 (17.08)	6.69 (46.06)
5	2.27 (1.26)	2.72 (0)	12.76 (12.37)
7	2.27 (1.15)	4.40 (0)	24.87 (38.61)
RUNX2 (day)			
1	2.55 (2.46)	4.20 (0)	8.85 (0)
3	2.55 (2.59)	5.11 (2.52)	12.27 (23.68)
5	1.96 (1.38)	4.12 (1.75)	9.23 (14.63)
7	2.71 (3.12)	3.21 (1.07)	11.03 (3.45)

Figure 1. Characterization of Osteogenically Induced hBMSC-EVs

EVs were isolated from the CM of hBMSCs under osteogenic medium (OM) or RUNX2 transcriptionally activated in basal medium (BM, RUNX2).

(A and B) EV size and charge. Representative size distribution profile highlighting the mean particle diameters (A); and EV size within the peak with main intensity (left axis) and charge (right axis), shown as the mean ± SEM (three donors, three technical replicates) (B).

(C) EV morphology. Representative atomic force micrographs (top) and graphical representation of individual EV size (a–c) (bottom).

(D) EV enrichment in CD9, CD63, and CD81 analyzed by flow cytometry. Representative histograms of labeled (open peak) and unlabeled (filled peak) EVs and the median fluorescence intensity ratio (median fluorescence intensity of the detected molecule divided by that of the non-labeled control), shown as the median (interquartile range [IQR]) (three donors, two technical replicates).

(E) EV yield in terms of normalized CD63-positive EVs (left axis) and normalized total EV protein (right axis), shown as the mean ± SEM (three donors, two and three technical replicates, respectively). **a** denotes significant differences compared with BM.

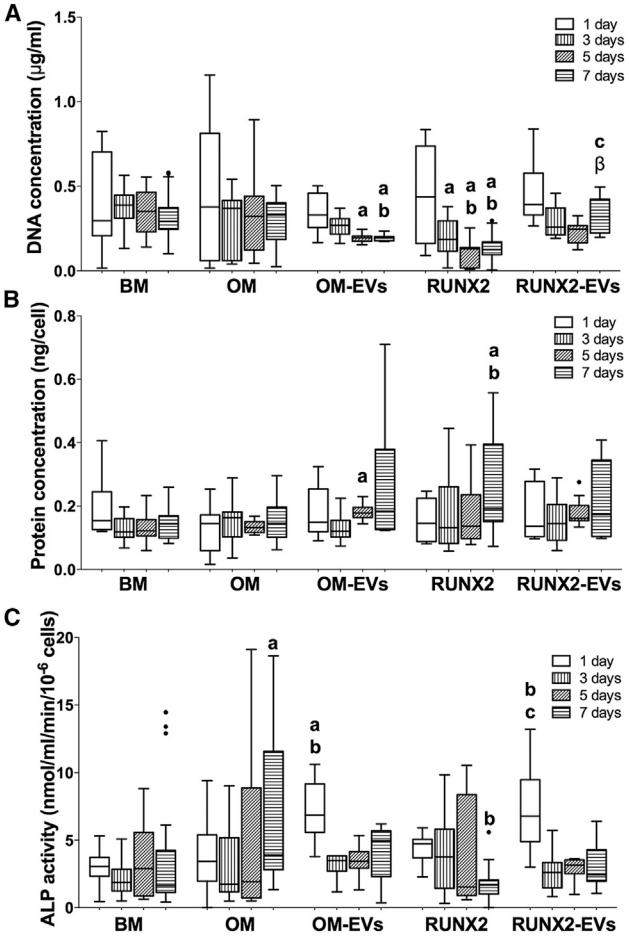

Figure 2. Effect of Osteogenically Induced hBMSC-EVs on the Biochemical Parameters of Homotypic Cells

EVs derived from hBMSCs under osteogenic medium (OM), OM-EVs, or RUNX2 transcriptionally activated in basal medium (BM), RUNX2-EVs, were transferred to uncommitted hBMSCs without further supplementation. Cell lysates (A) DNA concentration, (B) normalized protein, (C) normalized ALP activity are shown as Tukey boxplots (three donors, three technical replicates). The black dots denote outliers; letters denote significant differences compared with: **a**, BM; **b**, OM; **c**, RUNX2; **β**, OM-EVs.

integrin-binding sialoprotein (bone sialoprotein) (*IBSP*) (Figure 3E) were strongly upregulated (approximately 25-fold and 7-fold, respectively) in comparison with BM. Furthermore, RUNX2-EV-cultured hBMSCs showed lower mRNA *RUNX2* levels than those of parent cells stimulated to overexpress this gene, but similar to that observed in BM or OM (Figure 3A). As observed for OM-EVs, at early culture times, RUNX2-EVs induced the overexpression of *BMP2* by 3- to 8-fold (versus BM and OM) (Figure 3C) and that of *SP7* by 8-fold (versus BM) (Figure 3B), indispensable for progression onto the osteogenic lineage. Also consistent with osteogenic activation, the expression levels of *SPP1* (Figure 3D), and importantly those of bone γ-carboxyglutamate (gla) protein (osteocalcin) (*BGLAP*) (Figure 3F) were increased by 48- and 2-fold versus OM and/or BM, respectively. However, *IBSP* expression (Figure 3E) was only slightly increased on the first day of culture (versus BM, $p = 0.02$), whereas collagen type I alpha 1 (*COL1A1*) expression (Figure 3G) remained at the BM level although at higher levels than those observed for parent cells.

These results show that extracellular signaling derived from polymeric precipitated EVs obtained during hBMSCs osteogenic induction provides guidance for osteogenic lineage progression of homotypic cells.

DISCUSSION

Bone regenerative therapies have been challenged by the limited understanding of the induction of hBMSC fate. This hinders the clinical translation of the most promising strategies. For example, genetically modified cells raise safety, efficacy, and fate issues (Kumar et al., 2008); synthetic/recombinant factors, used at supra-physiological doses, are associated with severe side effects and high costs (Jakob et al., 2012); the CM concentration of biotherapeutics is low, at least for some applications, and contains medium contaminants, such as phenol red (Tran and Damaser, 2015).

Our study demonstrates that hBMSCs secrete vesicles with features of EVs that have osteoinductive potential. We showed that hBMSCs secrete a population of EVs heterogeneous in size, as noted earlier (Sokolova et al., 2011; Lobb et al., 2015; Van Deun et al., 2014). Although this can be attributed to the method of EV isolation (Lobb et al., 2015; Van Deun et al., 2014) or to sample aggregation, the sizes obtained (Figures 1A–1C) roughly fall within the range reported for hBMSC-EVs, 47–180 nm (Bian et al., 2014; Bruno et al., 2013). Consistent with MSCs expressing CD9 (Chen et al., 2010), CD63 (Stewart et al., 2003), and CD81 (Lee et al., 2009), EVs also showed these surface markers (Figures 1D and 1E), suggesting that they originated at the parent cell plasma membrane lipid rafts (Tan et al., 2013). Therefore, it is reasonable to accept that the parent cell source affects the EVs' surface proteins, their glycosylation or lipid composition, and consequently their charge. We found that the surface charge of hBMSC-EVs was relatively less negative (Figure 1B) than that reported for umbilical cord MSC-EVs, −52 mV (Sokolova et al., 2011). Furthermore, our data showed that the environmental stimuli affect the yield of EVs (Figure 1E) probably in parallel with cell activation (Figures 2A and 2B). This is in line with the oxygen-dependent placental secretion of MSC-EVs (Salomon et al., 2013). Due to their biophysical and biochemical properties, namely the size

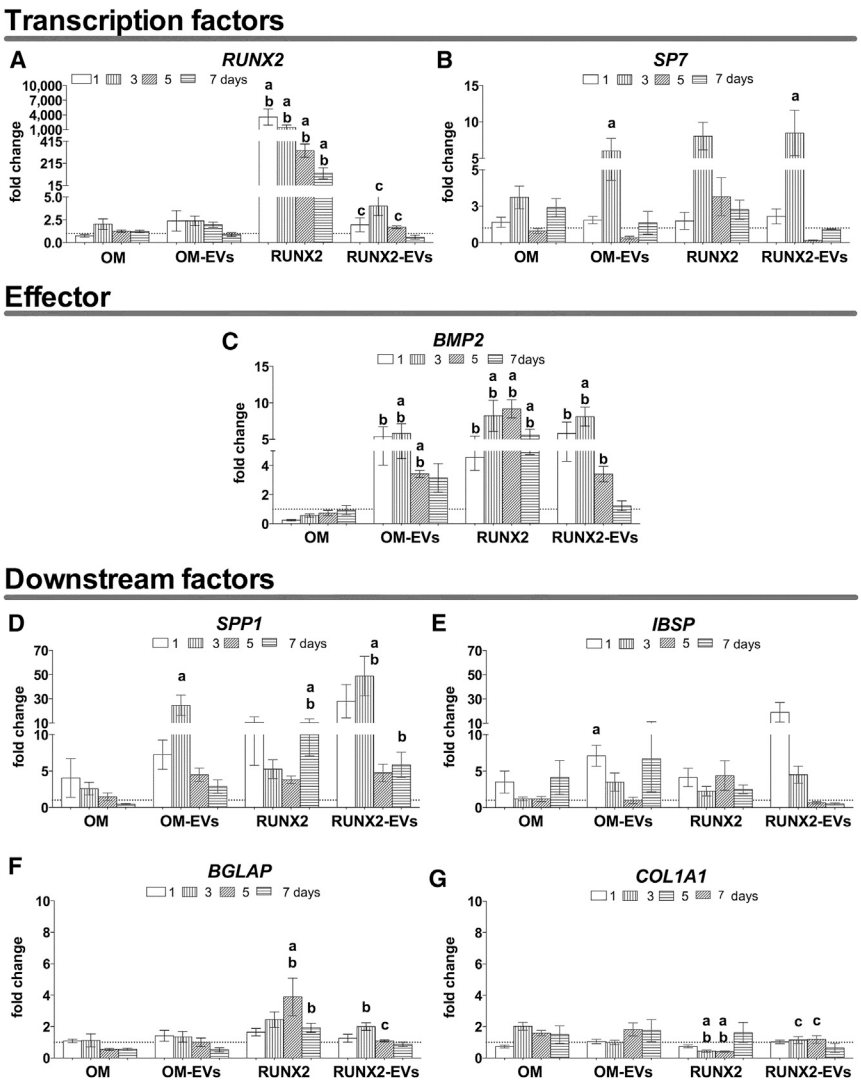

Figure 3. Effect of Osteogenically Induced hBMSC-EVs on Osteogenic Lineage-Related Markers of Homotypic Cells

EVs derived from hBMSCs under osteogenic medium (OM), OM-EVs, or RUNX2 transcriptionally activated in basal medium (BM), RUNX2-EVs, were transferred to uncommitted hBMSCs without further supplementation. BM was set as control. qPCR data for relative gene expression of (A and B) transcription factors, (C) effector, and (D–G) downstream factors, are shown as means ± SEM (three donors, three technical replicates). Letters denote significant differences compared with: **a**, BM; **b**, OM; **c**, RUNX2.

(Figures 1A–1C), EVs may interact differentially with cells. In general, the uptake of EVs is dose, time (Franzen et al., 2014), and recipient-cell (Feng et al., 2010) dependent, while the fate of the EV cargo varies with the particle subtype (Kanada et al., 2015). We indirectly showed that EVs added in concentrations comparable with those produced in vitro undergo uptake by hBMSCs, although the subtype and percentage of EVs being internalized was not determined.

The exogenous addition of osteogenically derived EVs outperformed the effect of current osteoinductive strategies in terms of the type and/or intensity of the signaling, with the early activation of the key osteogenic commitment genes *SP7* (Figure 3B) and *BMP2* (Figure 3C), considered necessary and sufficient to induce bone formation (Noel et al., 2004). In addition, EVs induced a transient upregulation of downstream matrix-associated genes and protein (Figures 3D, 3E, and 2C) that may be required to promote cell-cell and cell-matrix interactions and support long-term differentiation and mineralization (Langenbach and Handschel, 2013).

Notably, no major differences were noted between the exogenous addition of OM- or RUNX2-EVs, suggesting that the inherent cargo of hBMSC-EVs may also contribute to the observed effect. Indeed, the selective cargo of EVs derived from uncommitted hBMSCs suggests their involvement in the osteogenic differentiation. MSC-EVs were described to carry tRNA species putatively targeting the transcription factor *RUNX2* and *SOX11* (Baglio et al., 2015), miRNA, miR-22, that indirectly targets *RUNX2* (Baglio et al., 2015) and several proteins involved in the BMP, mitogen-activated protein kinase, transforming growth factor β, and Wnt pathways (Kim et al., 2012). Furthermore, our experimental design, comprising the

addition of a pool of OM-/RUNX2-EVs to hBMSCs, does not exclude the contribution of the EVs derived from recipient cells and a possible synergistic signaling.

Our results show the beneficial effects of cell-secreted factors, confirming that hBMSCs secrete EVs that are key players in the modulation of cell fate. We were able to identify and isolate unique factors that regulate the osteogenic commitment. Therefore, EVs are potential cell-free/secretome-based therapies for gene delivery applications that may circumvent the risks associated with current therapies and provide greater safety and efficacy benefits.

EXPERIMENTAL PROCEDURES

hBMSC Isolation and Culture

hBMSCs were obtained from three patients (aged 55, 68, and 71 years) after informed consent, as approved by the Ethical Committee of the Hospital Center of Alto Ave, Guimarães, under the Cooperation Agreement established between the 3B's Research Group, University of Minho and this hospital. hBMSCs were characterized and cultured using our standard protocols (Monteiro et al., 2014).

Osteogenic Commitment of Chemically and Genetically Induced hBMSCs

The following experiments were carried out using minimum essential medium alpha medium with fetal bovine serum depleted from EVs (Thery et al., 2006). The osteogenic commitment of adhered hBMSCs (passage 4; 750 cells/coverslip mm^2; 1 ml/well) was induced by chemical stimuli (BM with 10^{-8} M dexamethasone, 50 μg/ml ascorbic acid, and 0.01 M β-glycerophosphate; Sigma); or by genetic modulation (*RUNX2* cationic-lipid transfection in BM). The transfection mixture comprised 500 ng of plasmid DNA and a lipid-DNA ratio of 2× (Lipofectamine LTX with Plus Reagents, Alfagene, Life Technologies). After 5 hr the transfection mixture was replaced by 1 ml of BM. The transfection efficiency was evaluated by *GFP* reporter gene expression, showing a transient overexpression of *RUNX2* (Figure S1). See Supplemental Experimental Procedures for additional details. hBMSCs cultured in BM were set as control. For all the conditions, the CM was harvested at 1, 3, 5, and 7 days. The cells were rinsed, immersed in 1 ml of water or 0.8 ml of Tri-reagent (Sigma) and stored at −80°C.

Isolation of EVs

EVs were isolated from CM using a polymeric precipitation solution (ExoQuick-TC; System Biosciences, BioCat) according to the manufacturer's instructions. See Supplemental Experimental Procedures for additional details, including validation (Figure S2).

Characterization of Osteogenically Induced hBMSC-EVs

EV size was evaluated by DLS, charge by laser Doppler micro-electrophoresis (Malvern Nano ZS), and morphology by AFM (Dimension Icon, Bruker) at 15 μg of total protein/ml. EV total protein was evaluated by Micro BCA (Fisher Scientific) and CD63 by ELISA (EXOEL CD63, System Biosciences), according to the manufacturer's instructions; and CD9/63/81 by flow cytometry (Lasser et al., 2012). See Supplemental Experimental Procedures for additional details.

Transfer of Osteogenically Induced hBMSC-EVs into Uncommitted Homotypic Cells

Adhered hBMSCs (passage 4; 750 cells/coverslip mm^2; 1 ml/well) were fed with BM containing EVs derived from osteogenically induced hBMSCs after 1 day of culture, matching the seeding density. At days 1, 3, and 5 the recipient cells were fed with BM containing EVs derived from osteogenically induced hBMSCs, matching the seeding density, culture time, and stimuli. Cells were retrieved at 1, 3, 5, and 7 days and processed as the EV parent cells.

Cellular Biochemistry Analyses

Cell proliferation was evaluated by DNA quantification (Quant-iT PicoGreen dsDNA assay, Invitrogen, Alfagene), cellular protein by Micro BCA assay, according to the manufacturer's instructions; and alkaline phosphatase specific activity by a colorimetric assay (Monteiro et al., 2014). The number of hBMSCs was estimated based on an experimental standard curve (DNA = 0.0017 × cell number + 95.25, $R^2 = 0.98$).

Gene Expression Analyses

Total RNA was isolated and reverse transcribed into cDNA (qScript cDNA synthesis kit, Quanta BioSciences, VWR), followed by qPCR (PerfeCTa SYBR Green FastMix, Quanta BioSciences), according to the manufacturer's instructions. See Supplemental Experimental Procedures for additional details.

Statistical Analyses

Data normality was evaluated by the D'Agostino-Pearson test. A non-parametric Kruskal-Wallis test was applied followed by Dunn's test for multiple comparisons (GraphPad, version 6.0). Statistical significance was defined at $p < 0.01$.

SUPPLEMENTAL INFORMATION

Supplemental Information includes Supplemental Experimental Procedures, two figures, and one table and can be found with this article online at http://dx.doi.org/10.1016/j.stemcr.2016.01.001.

AUTHORS CONTRIBUTIONS

Study Conception and Design, M.M., A.M., R.L.R., N.M.N.; Acquisition of Data, M.M., D.R., A.M.; Analysis and Interpretation of Data, M.M., D.R., A.M., N.M.N.; Drafting of manuscript, M.M., A.M., N.M.N.; Critical Revision, N.M.N., R.L.R.

ACKNOWLEDGMENTS

The authors thank the financial support of QREN (RL1-ABMR-NORTE-01-0124-FEDER-000016 and RL3–TECT–NORTE-01-0124-FEDER-000020) co-financed by North Portugal Regional Operational Program (ON.2–O Novo Norte), under the NSRF, through the ERDF; the European Union's Seventh Framework Program (FP7/2007–2013), Grant No. REGPOT-CT2012-316331- POLARIS;

and the laboratory assistance of Elsa Ribeiro, Magda Graça, and Sónia Zacarias.

Received: October 7, 2015
Revised: January 4, 2016
Accepted: January 4, 2016
Published: February 25, 2016

REFERENCES

Akers, J.C., Gonda, D., Kim, R., Carter, B.S., and Chen, C.C. (2013). Biogenesis of extracellular vesicles (EV): exosomes, microvesicles, retrovirus-like vesicles, and apoptotic bodies. J. Neurooncol. *113*, 1–11.

Akyurekli, C., Le, Y., Richardson, R.B., Fergusson, D., Tay, J., and Allan, D.S. (2015). A systematic review of preclinical studies on the therapeutic potential of mesenchymal stromal cell-derived microvesicles. Stem Cell Rev. *11*, 150–160.

Baglio, S.R., Rooijers, K., Koppers-Lalic, D., Verweij, F.J., Perez Lanzon, M., Zini, N., Naaijkens, B., Perut, F., Niessen, H.W., Baldini, N., and Pegtel, D.M. (2015). Human bone marrow- and adipose-mesenchymal stem cells secrete exosomes enriched in distinctive miRNA and tRNA species. Stem Cell Res. Ther. *6*, 127.

Bian, S., Zhang, L., Duan, L., Wang, X., Min, Y., and Yu, H. (2014). Extracellular vesicles derived from human bone marrow mesenchymal stem cells promote angiogenesis in a rat myocardial infarction model. J. Mol. Med. *92*, 387–397.

Bruno, S., Collino, F., Deregibus, M.C., Grange, C., Tetta, C., and Camussi, G. (2013). Microvesicles derived from human bone marrow mesenchymal stem cells inhibit tumor growth. Stem Cells Dev. *22*, 758–771.

Chen, T.S., Lai, R.C., Lee, M.M., Choo, A.B., Lee, C.N., and Lim, S.K. (2010). Mesenchymal stem cell secretes microparticles enriched in pre-microRNAs. Nucleic Acids Res. *38*, 215–224.

Collino, F., Deregibus, M.C., Bruno, S., Sterpone, L., Aghemo, G., Viltono, L., Tetta, C., and Camussi, G. (2010). Microvesicles derived from adult human bone marrow and tissue specific mesenchymal stem cells shuttle selected pattern of miRNAs. PLoS One *5*, e11803.

Costa-Pinto, A.R., Correlo, V.M., Sol, P.C., Bhattacharya, M., Srouji, S., Livne, E., Reis, R.L., and Neves, N.M. (2012). Chitosan-poly(butylene succinate) scaffolds and human bone marrow stromal cells induce bone repair in a mouse calvaria model. J. Tissue Eng. Regen. Med. *6*, 21–28.

Ekstrom, K., Omar, O., Graneli, C., Wang, X., Vazirisani, F., and Thomsen, P. (2013). Monocyte exosomes stimulate the osteogenic gene expression of mesenchymal stem cells. PLoS One *8*, e75227.

Feng, D., Zhao, W.L., Ye, Y.Y., Bai, X.C., Liu, R.Q., Chang, L.F., Zhou, Q., and Sui, S.F. (2010). Cellular internalization of exosomes occurs through phagocytosis. Traffic *11*, 675–687.

Franzen, C.A., Simms, P.E., Van Huis, A.F., Foreman, K.E., Kuo, P.C., and Gupta, G.N. (2014). Characterization of uptake and internalization of exosomes by bladder cancer cells. Biomed. Res. Int. *2014*, 619829.

Heng, B.C., Cao, T., Stanton, L.W., Robson, P., and Olsen, B. (2004). Strategies for directing the differentiation of stem cells into the osteogenic lineage in vitro. J. Bone Miner. Res. *19*, 1379–1394.

Jaiswal, N., Haynesworth, S.E., Caplan, A.I., and Bruder, S.P. (1997). Osteogenic differentiation of purified, culture-expanded human mesenchymal stem cells in vitro. J. Cell. Biochem. *64*, 295–312.

Jakob, M., Saxer, F., Scotti, C., Schreiner, S., Studer, P., Scherberich, A., Heberer, M., and Martin, I. (2012). Perspective on the evolution of cell-based bone tissue engineering strategies. Eur. Surg. Res. *49*, 1–7.

Kanada, M., Bachmann, M.H., Hardy, J.W., Frimannson, D.O., Bronsart, L., Wang, A., Sylvester, M.D., Schmidt, T.L., Kaspar, R.L., Butte, M.J., et al. (2015). Differential fates of biomolecules delivered to target cells via extracellular vesicles. Proc. Natl. Acad. Sci. USA *112*, 1433–1442.

Karsenty, G., Kronenberg, H.M., and Settembre, C. (2009). Genetic control of bone formation. Annu. Rev. Cell Dev. Biol. *25*, 629–648.

Kim, H.S., Choi, D.Y., Yun, S.J., Choi, S.M., Kang, J.W., Jung, J.W., Hwang, D., Kim, K.P., and Kim, D.W. (2012). Proteomic analysis of microvesicles derived from human mesenchymal stem cells. J. Proteome Res. *11*, 839–849.

Kristensen, A.R., Gsponer, J., and Foster, L.J. (2013). Protein synthesis rate is the predominant regulator of protein expression during differentiation. Mol. Syst. Biol. *9*, 689.

Kumar, S., Chanda, D., and Ponnazhagan, S. (2008). Therapeutic potential of genetically modified mesenchymal stem cells. Gene Ther. *15*, 711–715.

Langenbach, F., and Handschel, J. (2013). Effects of dexamethasone, ascorbic acid and beta-glycerophosphate on the osteogenic differentiation of stem cells in vitro. Stem Cell Res. Ther. *4*, 117.

Lasser, C., Eldh, M., and Lotvall, J. (2012). Isolation and characterization of RNA-containing exosomes. J. Vis. Exp. *59*, e3037.

Lee, H.J., Choi, B.H., Min, B.H., and Park, S.R. (2009). Changes in surface markers of human mesenchymal stem cells during the chondrogenic differentiation and dedifferentiation processes in vitro. Arthritis Rheum. *60*, 2325–2332.

Lobb, R.J., Becker, M., Wen, S.W., Wong, C.S., Wiegmans, A.P., Leimgruber, A., and Moller, A. (2015). Optimized exosome isolation protocol for cell culture supernatant and human plasma. J. Extracell. Vesicles *4*, 27031.

Lötvall, J., Hill, A.F., Hochberg, F., Buzás, E.I., Di Vizio, D., Gardiner, C., Gho, Y.S., Kurochkin, I.V., Mathivanan, S., Quesenberry, P.J., et al. (2014). Minimal experimental requirements for definition of extracellular vesicles and their functions: a position statement from the International Society for Extracellular Vesicles. J. Extracell. Vesicles *3*, 26913.

Makridakis, M., Roubelakis, M.G., and Vlahou, A. (2013). Stem cells: insights into the secretome. Biochim. Biophys. Acta *1834*, 2380–2384.

Monteiro, N., Ribeiro, D., Martins, A., Faria, S., Fonseca, N.A., Moreira, J.N., Reis, R.L., and Neves, N.M. (2014). Instructive nanofibrous scaffold comprising runt-related transcription factor 2 gene delivery for bone tissue engineering. ACS Nano *8*, 8082–8094.

Noel, D., Gazit, D., Bouquet, C., Apparailly, F., Bony, C., Plence, P., Millet, V., Turgeman, G., Perricaudet, M., Sany, J., and Jorgensen, C.

(2004). Short-term BMP-2 expression is sufficient for in vivo osteochondral differentiation of mesenchymal stem cells. Stem Cells *22*, 74–85.

Nombela-Arrieta, C., Ritz, J., and Silberstein, L.E. (2011). The elusive nature and function of mesenchymal stem cells. Nat. Rev. Mol. Cell Biol. *12*, 126–131.

Roccio, M., Schmitter, D., Knobloch, M., Okawa, Y., Sage, D., and Lutolf, M.P. (2013). Predicting stem cell fate changes by differential cell cycle progression patterns. Development *140*, 459–470.

Salomon, C., Ryan, J., Sobrevia, L., Kobayashi, M., Ashman, K., Mitchell, M., and Rice, G.E. (2013). Exosomal signaling during hypoxia mediates microvascular endothelial cell migration and vasculogenesis. PLoS One *8*, e68451.

Sinha, K.M., and Zhou, X. (2013). Genetic and molecular control of osterix in skeletal formation. J. Cell. Biochem. *114*, 975–984.

Sokolova, V., Ludwig, A.K., Hornung, S., Rotan, O., Horn, P.A., Epple, M., and Giebel, B. (2011). Characterisation of exosomes derived from human cells by nanoparticle tracking analysis and scanning electron microscopy. Colloids Surf. B Biointerfaces *87*, 146–150.

Stewart, K., Monk, P., Walsh, S., Jefferiss, C.M., Letchford, J., and Beresford, J.N. (2003). STRO-1, HOP-26 (CD63), CD49a and SB-10 (CD166) as markers of primitive human marrow stromal cells and their more differentiated progeny: a comparative investigation in vitro. Cell Tissue Res. *313*, 281–290.

Tan, S.S., Yin, Y., Lee, T., Lai, R.C., Yeo, R.W., Zhang, B., Choo, A., and Lim, S.K. (2013). Therapeutic MSC exosomes are derived from lipid raft microdomains in the plasma membrane. J. Extracell. Vesicles *2*, 22614.

Thery, C., Amigorena, S., Raposo, G., and Clayton, A. (2006). Isolation and characterization of exosomes from cell culture supernatants and biological fluids. Curr. Protoc. Cell Biol. *Chapter 3*, Unit 3.22.

Torreggiani, E., Perut, F., Roncuzzi, L., Zini, N., Baglio, S.R., and Baldini, N. (2014). Exosomes: novel effectors of human platelet lysate activity. Eur. Cell. Mater. *28*, 137–151.

Tran, C., and Damaser, M.S. (2015). Stem cells as drug delivery methods: application of stem cell secretome for regeneration. Adv. Drug Deliv. Rev. *82-83*, 1–11.

Tsubota, S., Tsuchiya, H., Shinokawa, Y., Tomita, K., and Minato, H. (1999). Transplantation of osteoblast-like cells to the distracted callus in rabbits. J. Bone Joint Surg. Br. *81*, 125–129.

Ulsamer, A., Ortuno, M.J., Ruiz, S., Susperregui, A.R., Osses, N., Rosa, J.L., and Ventura, F. (2008). BMP-2 induces Osterix expression through up-regulation of Dlx5 and its phosphorylation by p38. J. Biol. Chem. *283*, 3816–3826.

Van Deun, J., Mestdagh, P., Sormunen, R., Cocquyt, V., Vermaelen, K., Vandesompele, J., Bracke, M., De Wever, O., and Hendrix, A. (2014). The impact of disparate isolation methods for extracellular vesicles on downstream RNA profiling. J. Extracell. Vesicles *3*, 24858.

Xu, J.F., Yang, G.H., Pan, X.H., Zhang, S.J., Zhao, C., Qiu, B.S., Gu, H.F., Hong, J.F., Cao, L., Chen, Y., et al. (2014). Altered MicroRNA expression profile in exosomes during osteogenic differentiation of human bone marrow-derived mesenchymal stem cells. PLoS One *9*, e114627.

Stem Cell Reports, Volume *6*

Supplemental Information

Extracellular Vesicles Derived from Osteogenically Induced Human Bone Marrow Mesenchymal Stem Cells Can Modulate Lineage Commitment

Margarida Martins, Diana Ribeiro, Albino Martins, Rui Luís Reis, and Nuno Meleiro Neves

SUPPLEMENTAL FIGURE 1

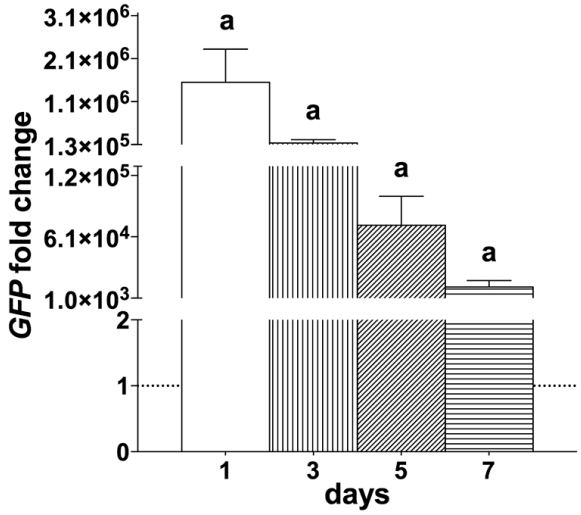

Figure S1. **hBMSCs RUNX2-transfection stability - related to Figure 2**
GFP expression, tagged to *RUNX2*, is shown as mean ± SEM (3 donors, with 3 technical replicates). BM was considered as calibrator at each time point and is indicated as a dashed line. **a**, denotes significant differences compared to BM.

SUPPLEMENTAL FIGURE 2

A

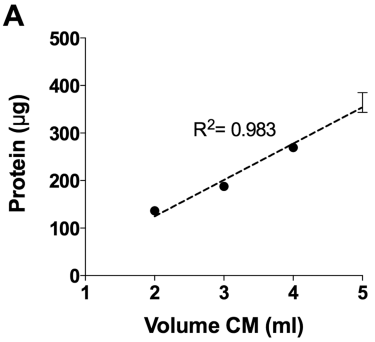

B

Experiment	EV-related protein amount (µg)	
	Spiked	Recovered
1	649.9 ± 33.9	558.8 ± 34.8
2	324.9± 17	324 ± 5.8

Figure S2. **Efficiency of the EVs enrichment method - related to Figure 1**
(**A**) Method linearity, showing a positive correlation between EVs protein and the conditioned medium (CM) volume. (**B**) Method recovery using high (experiment 1) and medium (experiment 2) amounts of EVs, showing a recovery efficiency ≥ 86%. The data is shown as mean ± SEM (n=3, with 3 technical replicates).

SUPPLEMENTAL TABLE

Table S1. Compilation of primers used for qPCR, related to Figure 3

Name	Primer sequence 5'-3' Forward/ reverse	Tm (°C)	Product size (bp)	Sequence Reference (NCBI)
BGLAP	GTGCAGAGTCCAGCAAAGG TCAGCCACTCGTCACAGC	59.4	549	DQ007079.1
BMP2	TGAATCAGAATGCAAGCAGG TCTTTTGTGGAGAGGATGCC	56.3	250	NM_001200.2
COL1A1	AAGAACCCCAAGGACAAGAG GTAGGTGATGTTCTGGGAGG	58.4	159	NM_000088.3
GFP	AACACCCGCATCGAGAAGTA CTTGAAGTGCATGTGGCTGT	57.3	279	pCMV6-eGFP Origene
GAPDH	ACAGTCAGCCGCATCTTCTT GACAAGCTTCCCGTTCTCAG	58.4	308	NM_002046.4
IBSP	ACTGAGCCTGTGTCTTGAAA CTTCCAACAGCCAATCACTG	56.3	102	AH002985.1
RUNX2	TTCCAGACCAGCAGCACTC CAGCGTCAACACCATCATTC	58.1	242	NM_001145920.1
SP7	CCCTTTACAAGCACTAATGG ACACTGGGCAGACAGTCAG	57.1	216	NM_001173467.1
SPP1	CCCACAGACCCTTCCAAGTA GGGGACAACTGGAGTGAAAA	58.4	244	AF052124.1

Tm, melting temperature; bp, base pairs

SUPPLEMENTAL EXPERIMENTAL PROCEDURES

RUNX2 plasmid construct

Genetically- induced hBMSCs osteogenic commitment

The commercial available plasmid pCMV6-AN-GFP (PS100019, Origene, USA; 6.6 kb) was modified to express runt-related transcription factor 2 gene (*RUNX2*, NM_001024630). This vector carries the cytomegalovirus (CMV) promoter, the human growth hormone polyA signal downstream the insert, the ColE1 ori for replication in bacteria, the Simian vacuolating virus 40 ori for replication in mammalian cells, the f1 ori for the recovery of single-stranded plasmids and an ampicillin resistance gene for plasmid selection purposes in *Escherichia coli*. The open reading frame cloned in this vector is expressed with a tagged turbo Green Fluorescent Protein (GFP). Competent *E. coli* DH5α grown at 37°C on Luria-Bertani medium (Gibco) supplemented with ampicillin (Sigma, Spain) (150 μg/mL) was used as host for the *RUNX2* plasmid amplification after heat shock transformation (Sambrook and Russell, 2001). Plasmid DNA isolation was performed using the Plasmid Midi kit (Qiagen, IZASA, Portugal) according to the manufacturer's instructions. Determination of the plasmid DNA concentration and purity was performed by microspectrophotometry (NanoDrop 1000, Thermo Scientific, Portugal).

For the genetically induced commitment, cationic-lipid transfection (Lipofectamine LTX with Plus Reagents, Life Technologies, Alfagene) was used. The transfection mixture was composed by 500 ng of plasmid DNA and a lipid to DNA ratio of 2 ×. The lipid/DNA complexes formed in Opti-MEM were added to 1 h adhered cells. After 5 h, the cells were rinsed with phosphate buffer saline (PBS; Sigma) and fed with 1 ml of BM. The transfection efficiency was evaluated by the quantitative real-time polymerase chain reaction (qPCR) *GFP* reporter gene expression (Figure S1). hBMSCs cultured in BM were set as control.

Isolation of EVs

To exclude large cell debris, membranes and/or apoptotic bodies the conditioned medium (CM) was filtered (pore size 0.22 μm) (Thery et al., 2006). EVs were isolated from the CM using a polymeric precipitation solution (ExoQuick-TC; System Biosciences, BioCat GmbH, Germany). This method is based on the trapping of EVs, under salt conditions at 4°C. EVs are pelleted by low-speed centrifugation. Upon resuspension of the recovered sample the residual polymer is diluted and the EVs are liberated (Peterson et al., 2015). One ml of solution was mixed with 5 ml of CM and incubated overnight at 4°C. After centrifugation at room temperature, 1500 × *g*, 30 min (Eppendorf, Fisher Scientific, Portugal), the supernatant was discarded and the tubes were centrifuged at 1500 × *g*, 5 min. The pelleted EVs were resuspended in phosphate buffered saline (PBS) for all the EVs characterization assays but the CD63 protein ELISA assay, for which exosome binding buffer (EXOEL CD63; System Biosciences) was used; or in BM for the "Transfer of osteogenically committed hBMSCs-EVs into uncommitted homotypic cells" assays, and used fresh.

For control experiments, BM was processed as the CM and after centrifugation no pellet was detected, excluding potential contamination by fetal bovine serum FBS-EVs. The EVs isolation procedure was validated using a pool of CM obtained from hBMSCs cultured for 7 days. To evaluate the linearity, a variable amount of CM (2 to 5 ml) in a final volume of 5 ml was mixed with ExoQuick solution (Figure S2A). To evaluate the recovery, two known amounts of EVs total protein (corresponding to high, 200% and medium, 100 % amounts) were added to 5 ml of BM and mixed with ExoQuick solution (Figure S2B). EVs were isolated as described above. The pellets were resuspended in 500 μl of PBS and the EVs enrichment was evaluated in terms of total protein recovered that can give a rough indication of the EVs amount (Webber and Clayton, 2013). Total protein (in μg) was calculated as the protein concentration × volume after processing. Percentage recovery was calculated as the protein amount recovered divided by the protein amount spiked × 100.

Characterization of osteogenically induced hBMSCs-EVs

Size and charge

Size was evaluated by dynamic light scattering (DLS) in 1 cm polystyrene cells and ζ- potential by Laser Doppler micro-electrophoresis in folded capillary cells using a Malvern Nano ZS (He–Ne laser source; λ= 633 nm; Malvern, Portugal) under a fixed angle of 173°. DLS measures the changes in the light scattered from a laser due to the Brownian motion of EVs populations (ranging from 0.6 nm and 6 μm) in solution along time. This assumes that the particles are spherical and depends on the solvent, temperature, refractive index of the EVs and of the solvent and EVs size. The relative size distribution is obtained through the equipment software algorithm that correlates light intensity fluctuations with particle size. It also provides an estimate of the width of the size distribution- the polydispersity index-

that ranges from 0 (monodisperse) to 1 (very broad distribution) (van der Pol et al., 2010). The zeta potential is measured using Laser Doppler Electrophoresis, which measures light scattered by EVs (ranging from 5 nm and 10 μm) when an electric field is applied to the solution. All the measurements were performed using filtered solutions composed of EVs (15 μg of total protein) in 1 ml of PBS at 37°C.

Morphology
EVs (15 μg of total protein/ ml of PBS) were adsorbed for 30 min into coverslips (Sarsted, Germany), rinsed with ultrapure water twice and air-dried. The samples were analyzed by atomic force microscopy (Dimension Icon, Bruker**,** Japan) using the ScanAsyst Imaging Mode, in air.

Total protein
The quantification of EVs' total protein was performed using the Micro BCA Protein Assay kit (Fisher Scientific, Portugal). The samples were diluted in PBS. The protein concentration was calculated using a standard curve relating the concentration of bovine serum albumin (BSA; ranging from 2 to 40 μg/mL) to the absorbance measured at 562 nm on a microplate reader (Synergie HT, Bio-Tek, Alfagene). The values recorded for the total protein in each sample were adjusted for the CM volume and standardized against the cell number of progenitor cells and days in culture.

Surface markers
First, the evaluation of EVs' CD9/CD63/CD81 markers was performed by flow cytometry. CD63-beads were prepared by overnight incubation at room temperature of 4% (w/v) 4 μm beads aldehyde/sulfate latex (Molecular Probes, Alfagene) with anti-human CD63 (BD Biosciences) in 2-(*N*-morpholino)ethanesulfonic acid (Sigma) buffer pH6. EVs were incubated with PBS washed CD63-beads (150 μg EVs/ 5×10^5 CD63-beads) overnight at 4°C. After glycine (Sigma) block (final concentration 100 μM) and wash with 0.5% BSA (w/v) in PBS the bead-sample complexes were incubated with CD9- fluorescein isothiocyanate (FITC, 0.06 μg), CD63 allophycocyanin (APC, 0.22 μg), or CD81 phycoerythrin (PE, 0.08 μg) (all from BD Biosciences, Enzifarma, Portugal) for 40 min at 4°C under gentle agitation in 0.5% BSA in PBS. After washing, the samples were acquired on a FACsCalibur Flow Cytometer (BD Biosciences) at low flow rate. Offline data analysis was performed on FlowJo. From the dot plot representation of forward and side scatter, single EVs-CD63-beads were gated for fluorescence analysis (10,000 events per gated population). This population was compared to unlabeled controls.
Second, the quantification of CD63 positive EVs was performed using the EXOEL CD63 kit (System Biosciences). This is an ELISA based on the colorimetric detection of the specific interaction between enzyme labeled CD63 and EVs immobilized on a microtiter plate. The quantitative results (number of EVs particles) were obtained using a protein standard curve relating the amount of EVs (ranging from 1.35×10^{10} to 2.1×10^8 particles) to the absorbance measured at 450 nm on a microplate reader (Synergie HT). The values recorded for the number of EVs particles in each sample were adjusted for the CM volume and standardized against the cell number of progenitor cells and days in culture.

Gene expression analyses
RNA was extracted from Tri-reagent derived cell lysates according to manufacturer's instructions. The RNA pellets were solubilized in water RNase/DNase free (VWR, Portugal). The RNA concentration was determined by microspectrophotometry (NanoDrop 1000). The cDNA synthesis was performed using the qScript cDNA synthesis kit (Quanta BioSciences, VWR) with 100 ng RNA template in a final volume of 20 μl. Cycling was as follows: 1 cycle at 22°C, 5 min; 1 cycle at 42°C, 30 min; 1 cycle at 85°C, 5 min. The amplification of the target cDNA was performed using the PerfeCTa SYBR Green FastMix (Quanta BioSciences) with 1 μL of cDNA, 125 nM of each primer (Table S1) in a final volume of 20 μl. Real time-PCR cycling was as follows: 1 cycle at 95°C, 2 min; 44 cycles at 95°C, 10 s/ gene annealing temperature (Table S1), 30 s/72 °C, 30 s; followed by dissociation curve analysis. All the reactions were carried out on a PCR cycler Mastercycler Realplex (Hamburg, Germany). The transcripts expression data were normalized to the housekeeping gene glyceraldehyde-3-phosphate dehydrogenase (*GAPDH*) in each sample. The quantification was performed according to the Livak method ($2^{-\Delta\Delta Ct}$ method), considering the BM condition for each time point as a calibrator (threshold = 1).

SUPPLEMENTAL REFERENCES
Peterson, M.F., Otoc, N., Sethi, J.K., Gupta, A., and Antes, T.J. (2015). Integrated systems for exosome investigation. Methods. *87*: 31–45.

Sambrook J., Russell D.W., (2001) Molecular cloning - a laboratory manual, 3rd ed., Cold Spring Harbor Laboratory Press, Cold Spring Harbor, New York.
Van Der Pol, E., Hoekstra A.G., Sturk, A., Otto, C., van Leeuwen, T.G., Nieuwland R. (2010) Optical and non-optical methods for detection and characterization of microparticles and exosomes. J. Thromb. Haemost. *8*, 2596-2607.
Webber, J., and Clayton, A. (2013). How pure are your vesicles? J. Extracell. Vesicles. *2*. 19861.